Metallomics, 16, 2024, mfae007
https://doi.org/10.1093/mtomcs/mfae007
Advance access publication date: 29 January 2024
Paper

Loss of SLC30A10 manganese transporter alters expression of neurotransmission genes and activates hypoxia-inducible factor signaling in mice

Anna Warden[1], R. Dayne Mayfield[1], Kerem C. Gurol[2], Steven Hutchens[2], Chunyi Liu[2,3,*] and Somshuvra Mukhopadhyay[2,*]

[1]Waggoner Center for Alcohol and Addiction Research, The University of Texas at Austin, Austin, TX 78712, USA, [2]Division of Pharmacology & Toxicology, College of Pharmacy; and Institute for Neuroscience, The University of Texas at Austin, Austin, TX 78712, USA and [3]Current address: Institute for Brain Science and Disease, Chongqing Medical University, Chongqing, China; and Key Laboratory of Major Brain Disease and Aging Research (Ministry of Education), Chongqing Medical University, Chongqing, China
*__Correspondence:__ Division of Pharmacology and Toxicology, University of Texas at Austin, 107 W. Dean Keeton, Austin, TX 78712, USA.
E-mail: ylcy2020@outlook.com; Division of Pharmacology and Toxicology, University of Texas at Austin, 3.510 BME, 107 W. Dean Keeton, Austin, TX 78712, USA.
Tel: +512-471-5873; E-mail: som@austin.utexas.edu

Abstract

The essential metal manganese (Mn) induces neuromotor disease at elevated levels. The manganese efflux transporter SLC30A10 regulates brain Mn levels. Homozygous loss-of-function mutations in *SLC30A10* induce hereditary Mn neurotoxicity in humans. Our prior characterization of *Slc30a10* knockout mice recapitulated the high brain Mn levels and neuromotor deficits reported in humans. But, mechanisms of Mn-induced motor deficits due to *SLC30A10* mutations or elevated Mn exposure are unclear. To gain insights into this issue, we characterized changes in gene expression in the basal ganglia, the main brain region targeted by Mn, of *Slc30a10* knockout mice using unbiased transcriptomics. Compared with littermates, >1000 genes were upregulated or downregulated in the basal ganglia sub-regions (i.e. caudate putamen, globus pallidus, and substantia nigra) of the knockouts. Pathway analyses revealed notable changes in genes regulating synaptic transmission and neurotransmitter function in the knockouts that may contribute to the motor phenotype. Expression changes in the knockouts were essentially normalized by a reduced Mn chow, establishing that changes were Mn dependent. Upstream regulator analyses identified hypoxia-inducible factor (HIF) signaling, which we recently characterized to be a primary cellular response to elevated Mn, as a critical mediator of the transcriptomic changes in the basal ganglia of the knockout mice. HIF activation was also evident in the liver of the knockout mice. These results: (i) enhance understanding of the pathobiology of Mn-induced motor disease; (ii) identify specific target genes/pathways for future mechanistic analyses; and (iii) independently corroborate the importance of the HIF pathway in Mn homeostasis and toxicity.

Keywords: SLC30A10, transporter, manganese, ZnT10, transcriptomics, parkinsonism, dopamine, trace element homeostasis, trace element transporter

Graphical abstract

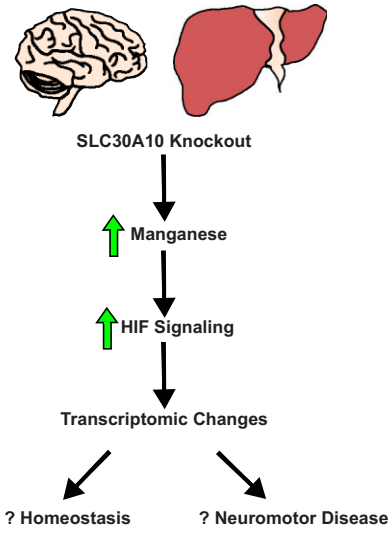

Mn-induced transcriptomic changes in brain and liver of *Slc30a10* knockout mice.

Received: October 10, 2023. **Accepted:** January 16, 2024

Introduction

The essential metal manganese (Mn) induces neurotoxicity at elevated levels.[1] Mn neurotoxicity has historically been reported in occupationally exposed adults who develop a parkinsonian-like motor disease.[1] More recently, elevated exposure to Mn from environmental sources (e.g. drinking water, air, soil, etc.) has emerged as an important public health problem, particularly in the developmentally sensitive early-life stages of infancy, childhood, and adolescence.[1] Environmental Mn exposure in these critical life stages is associated with motor dysfunction (e.g. in motor coordination, skilled motor function, tremor intensity, postural stability, etc.) as well as executive function deficits,[1–6] and neurological deficits induced by developmental Mn exposure may persist into later-life stages.[1] In addition to elevated exposure, Mn neurotoxicity may also occur in individuals with compromised liver function (e.g. alcoholic cirrhosis) because excretion via the liver (and intestines) is a major pathway that regulates brain Mn.[7–9] Finally, homozygous loss-of-function mutations in the Mn transporters SLC30A10 or SLC39A14 induce hereditary Mn neurotoxicity in humans.[7,10–12] Despite the clinical relevance, understanding of the mechanisms of Mn neurotoxicity is limited, which has hindered progress toward the development of effective therapeutics.

A major focus of ongoing research is to understand the molecular bases of Mn-induced motor disease because: (i) excess Mn primarily accumulates in the basal ganglia in the brain,[1] which controls movement[13,14]; (ii) motor dysfunction is a primary manifestation of Mn neurotoxicity[1]; and (iii) exposure to elevated Mn may also increase the risk of developing Parkinson's disease.[15] Recent rodent studies indicate that elevated brain Mn levels induce a deficit in neurotransmitter release, particularly dopamine release,[16–18] which is expected to impact synaptic activity and motor function. A possible mechanism by which increased brain Mn may induce deficits in neurotransmitter release and synaptic function is changes in gene expression. In the current study, we addressed this possibility using an unbiased transcriptomics approach.

Our studies used the full-body *Slc30a10* knockout mouse model, which we previously developed and reported.[9,19,20] SLC30A10 is a critical Mn efflux transporter that regulates brain Mn levels.[1,7–9,16,19–23] Humans with homozygous loss-of-function mutations in *SLC30A10* develop hereditary Mn neurotoxicity with elevated brain Mn levels and parkinsonism-dystonia.[1,10,12] Full-body *Slc30a10* knockout mice recapitulate the high brain Mn levels and motor deficits observed in humans.[9,19,20,24] Use of the well-characterized *Slc30a10* knockout mouse model: (i) precluded Mn dosing in the mice, thereby eliminating a potential source of variation; (ii) allowed us to add a rescue component to the study with reduced Mn chow, which rescues the Mn toxicity phenotype of the full-body *Slc30a10* knockout mice[9,19]; and (iii) was expected to provide data relevant to hereditary as well as exposure-induced Mn neurotoxicity. Our findings show that expression of critical genes that regulate neurotransmitter release, synaptic function, and membrane trafficking are altered in the basal ganglia of the *Slc30a10* knockout mice. We further identify signaling via the hypoxia-inducible factor (HIF) pathway, which we recently characterized as the primary homeostatic response to elevated Mn levels,[25] to be a critical upstream regulator of the transcriptomic changes in the *Slc30a10* knockout mice. These results provide new insights into the biology of Mn-induced motor disease and identify a set of critical genes and pathways that may directly modulate Mn neurotoxicity for future mechanistic analyses.

Results

Slc30a10 knockout mice exhibit changes in the expression of genes that regulate synaptic function and neurotransmitter release in the substantia nigra

To analyse Mn-induced gene expression changes that may influence motor function in an unbiased manner, we performed Tag-seq analyses in basal ganglia tissue collected from ~1-mo-old littermate control or full-body *Slc30a10* knockout mice fed regular rodent chow (~84 μg Mn/g chow). We previously reported that knockouts on regular rodent chow display: (i) ~20-fold higher brain Mn levels compared with littermates at ~1 mo of age; and (ii) motor deficits (analysed at ~5–6 wk of age).[9,19] To increase the sensitivity of our study, we separated the three major sub-regions of the basal ganglia (caudate putamen, globus pallidus, and substantia nigra[13,14]) using a brain punch technique and performed transcriptomic analyses in all three regions independently.

In the substantia nigra of the knockouts, ~60–70 genes were upregulated or downregulated (Fig. 1A–C; Supplementary Table S1). As expected, expression of *Slc30a10* in the knockouts was negligible (Fig. 1B; Supplementary Table S1). Major upregulated pathways included regulation of synaptic transmission (glutamatergic) and several aspects of neuronal physiology (e.g. neuronal apoptosis/death, projection development, migration, etc.) (Fig. 1D and E; Supplementary Tables S1 and S2). Expression of notable genes that were upregulated in these pathways included the metabotropic glutamate receptor *Grm2* and several modulators of membrane trafficking and cytoskeletal organization, such as *Clip1*, which links endocytic vesicles to microtubules; the actin-capping gene *Tmod1*; and the cadherin family member *Cdh23* (Table 1).[26] Expression of several canonical hypoxia/HIF-regulated genes were also upregulated (Fig. 1D and E; Table 1),[26–31] providing evidence of HIF activation. Genes regulating synaptic transmission and neurotransmitter release were strongly represented in the downregulated pathways as well (Fig. 1F and G; Supplementary Tables S1 and S2). In particular, expression of multiple genes that regulate GABAergic neurotransmission were downregulated (e.g. *Gad1* and *Gad2*, which are involved in GABA synthesis; *Slc32a1*, involved in GABA uptake into synaptic vesicles; and *Abat*, which catabolizes GABA) (Fig. 1F and G; Table 1).[26] Furthermore, expression of a critical regulator of dopaminergic neurotransmission that is disrupted in Parkinson's disease, *Sv2c*,[32] was also downregulated (Table 1). Expression of genes regulating several metabolic pathways and oxidative phosphorylation were downregulated as well (Supplementary Tables S1 and S2), suggestive of widespread physiological disruption in the knockouts. Overall, expression changes in critical regulators of neurotransmitter release and synaptic function are an important component of the transcriptomic profile of the substantia nigra of *Slc30a10* knockout mice.

Changes in genes regulating synaptic and neurotransmitter function also occur in the caudate putamen of the *Slc30a10* knockout mice

In the caudate putamen of the knockouts, expression of ~600 genes were upregulated and ~200 downregulated (Fig. 2A–C; Supplementary Table S1), and expression of *Slc30a10* was negligible (Fig. 2B; Supplementary Table S1). Important upregulated pathways included synaptic organization, transmission, and assembly, neuronal projection, and axon development (Fig. 2D and E; Supplementary Table S2). Critical genes with upregulated expression in these pathways included several regulators of

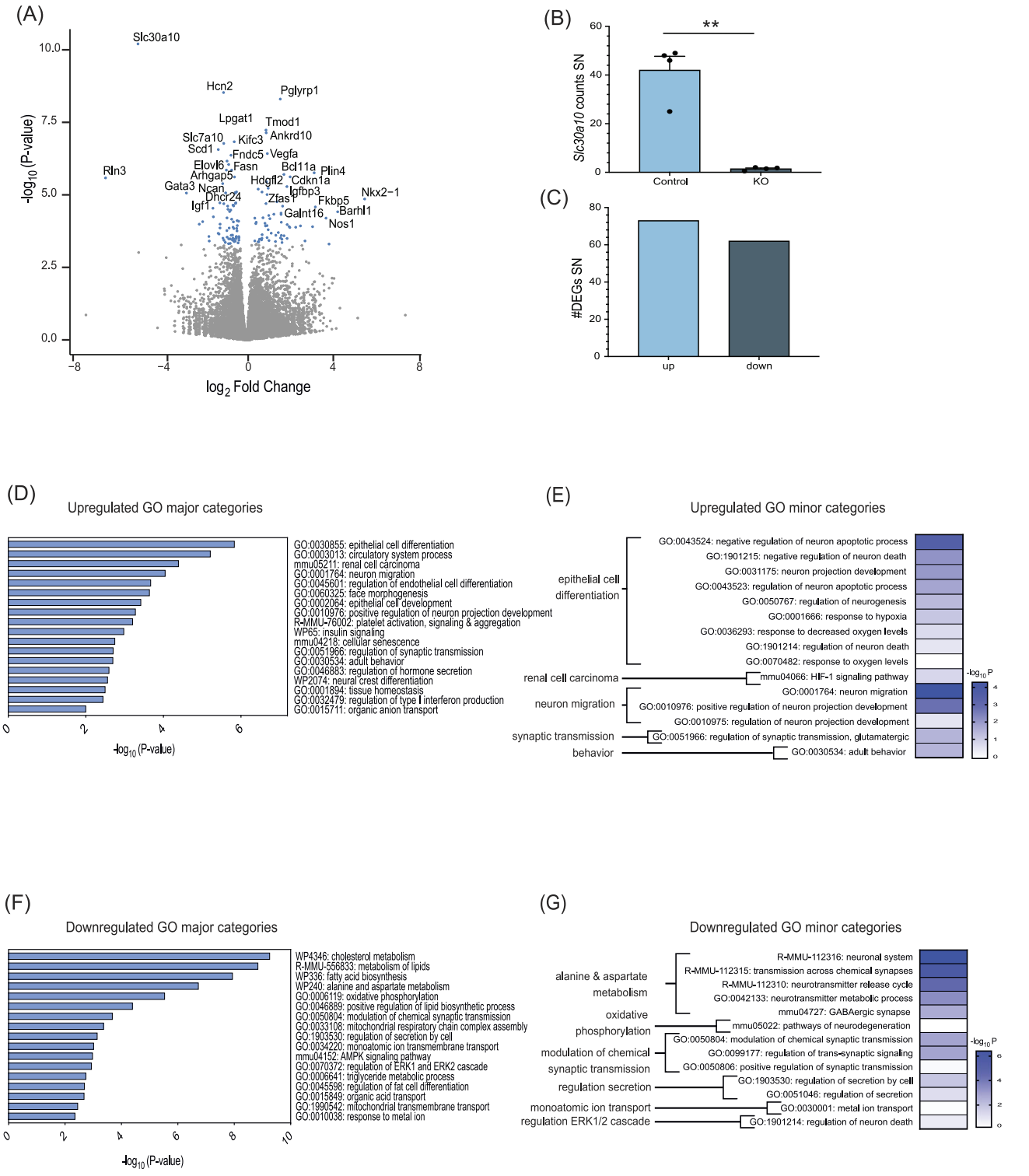

Fig. 1 Expression of synaptic/neurotransmission and HIF/hypoxia-dependent genes are altered in the substantia nigra of *Slc30a10* knockout mice on regular rodent chow. (A) Volcano plot showing $\log_2$ fold change against $-\log_{10}$ P-value for the main effect of littermate control vs. *Slc30a10* knockout mice in the substantia nigra (SN). Differentially expressed genes (DEGs) ($P_{adj} < 0.05$) are shown as blue dots. The top DEGs are labeled. (B) *Slc30a10* expression in the SN of *Slc30a10* knockout (KO) or *Slc30a10*$^{fl/fl}$ littermate control mice. (C) Number of upregulated (62) and downregulated (74) DEGs in the SN of *Slc30a10* knockout mice ($P_{adj} < 0.05$). Pathway enrichment and gene ontology analyses for upregulated SN DEGs of *Slc30a10* knockout mice showing (D) major categories and (E) minor categories of enrichment as a function of $-\log_{10}$ (P-value). Pathway enrichment and gene ontology analyses for downregulated SN DEGs of *Slc30a10* knockout mice showing (F) major categories and (G) minor categories of enrichment as a function of $-\log_{10}$ (P-value). $N = 4$ mice per genotype. $^{**}P < 0.01$.

Table 1. List of major differentially expressed genes in *Slc30a10* knockout mice compared with littermate controls on regular or reduced Mn chow.[a]

Substantia Nigra			
Gene	**Fold change (regular chow)**	**Fold change (low Mn chow)**	**Function of protein**
Grm2	2.73	1.08	Metabotropic glutamate receptor
Clip1	0.47	0.11	Links endocytoic vesicles to microtubules
Tmod1	0.93	0.72	Actin-capping protein
Cdh23	1.90	−0.21	Cadherin superfamily member
Vegfa	0.99	0.56	Canonical Hif-dependent gene
Kdr	1.06	0.43	Vegf receptor; Induced by hypoxia
Hif3a	1.63	1.51	Hifα isoform
Slc2a1	1.03	0.53	Hif-dependent glucose transporter (Glut1)
Cdkn1a	2.04	0.91	Hif-dependent cell cycle regulator (p21)
Gad1	−1.20	−0.36	GABA biosynthesis enzyme
Gad2	−0.96	−0.14	GABA biosynthesis enzyme
Slc32a1	−1.21	−0.08	GABA vesicular transporter (Vgat)
Abat	−0.60	−0.07	GABA catabolism
Gria4	−0.66	−0.18	Ionotropic glutamate receptor
Ncs1	−0.56	−0.12	Neuronal Ca sensor
Sv2c	−1.20	−0.09	Regulates dopaminergic neurotransmission
Caudate Putamen			
Gene	**Fold change (Regular Chow)**	**Fold Change (Low Mn Chow)**	**Function of protein**
Grm2	2.01	NA	Metabotropic glutamate receptor
Adra2a	1.90	NA	Adrenergic receptor
Chrm3	0.83	−0.31	Muscarinic cholinergic receptor
Htr1a	1.92	NA	Serotonin receptor
Htr2a	1.23	0.36	Serotonin receptor
Doc2a	1.60	NA	Ca-dependent neurotransmitter release
Glul	0.55	0.16	Glutamate detoxification
Syt13	1.02	−0.11	Synaptogamin; membrane trafficking
Syt17	1.16	NA	Synaptotagmin; membrane trafficking
Stx1a	0.83	−0.12	Syntaxin; membrane trafficking; synaptic exocytosis
Stx3	0.54	−0.24	Syntaxin; membrane trafficking
Cplx3	4.77	NA	SNARE binding
Cadps2	1.71	0.27	Synaptic exocytosis
Vegfa	0.95	0.40	Canonical HIF-dependent gene
Kdr	1.26	0.63	Vegf receptor; Induced by hypoxia
Hif3a	1.62	0.95	Hifα isoform
Epas1 (Hif2a)	0.53	0.19	Hifα isoform
Slc7a5	1.10	1.08	Thyroid hormone transporter
Slc6a9	−1.11	−0.56	Glycine transporter
Syt3	−0.57	NA	Synaptogamin; membrane trafficking
Syt9	−1.22	−0.11	Synaptotagmin; membrane trafficking
Ston2	−0.69	0.27	Endocytosis; synaptic vesicle recycling
Globus Pallidus			
Gene	**Fold change (Regular Chow)**	**Fold Change (Low Mn Chow)**	**Function of protein**
Stxbp5	0.68	−0.02	Syntaxin binding protein; SNARE formation
Vegfa	1.03	0.59	Canonical Hif-dependent gene
Kdr	1.81	0.69	Vegf receptor; Induced by hypoxia
Hif3a	2.13	0.98	Hifα isoform
Slc16a2	0.87	−0.03	Thyroid hormone transporter
Slc7a5	0.98	0.89	Thyroid hormone transporter
Slco1c1	0.94	0.34	Thyroid hormone transporter
Med16	0.61	−0.19	Thyroid hormone receptor binding activity
Slc6a11	−1.60	0.12	GABA transporter
Grin3a	−1.28	0.10	Ionotropic glutamate receptor
Gria4	−0.57	−0.05	Ionotropic glutamate receptor

[a]Log_2 fold change for expression change in knockouts compared with littermates is indicated for each gene. NA, not applicable.

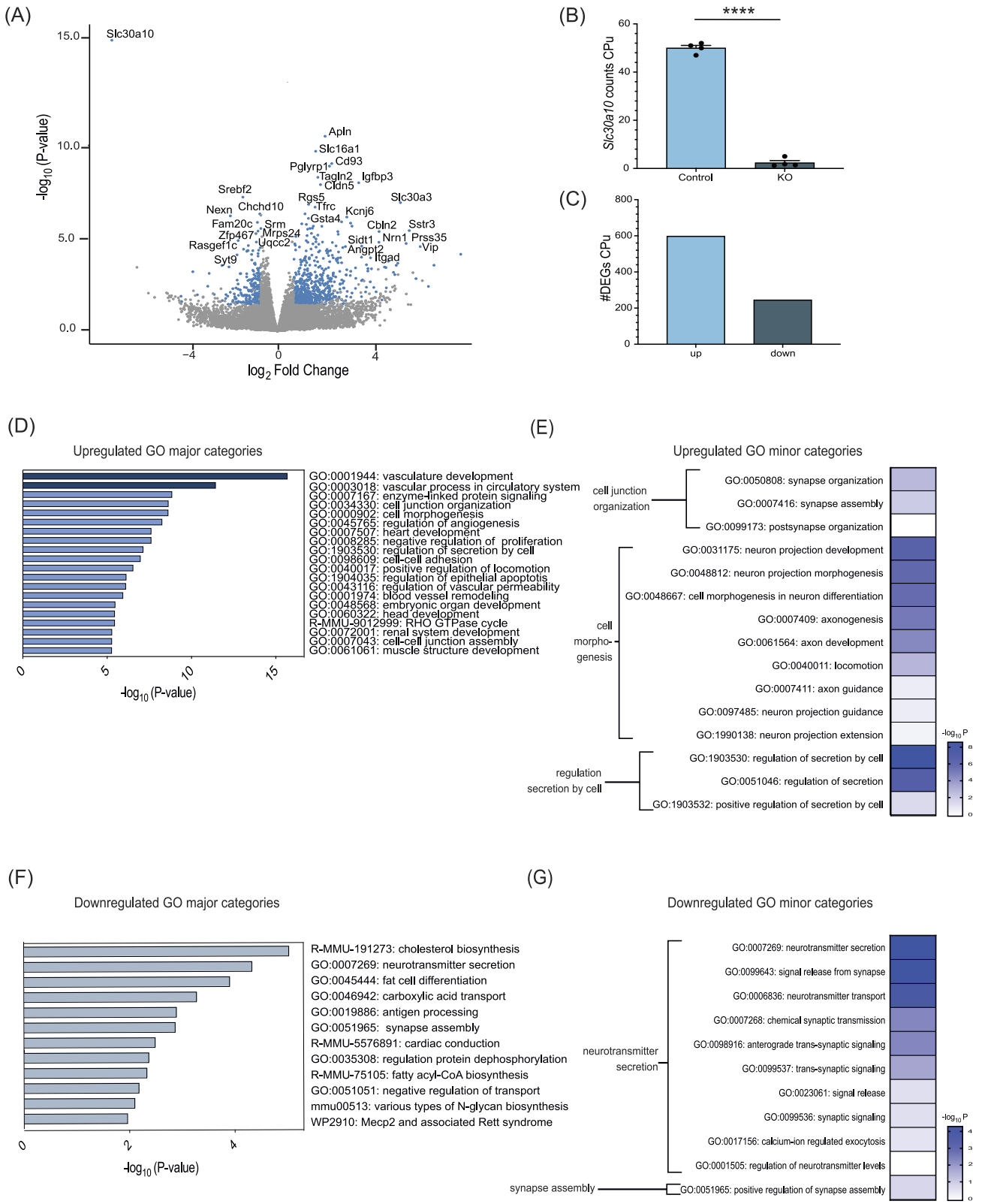

Fig. 2 *Slc30a10* knockout mice on regular rodent chow exhibit changes in expression of neuronal regulators and HIF/hypoxia-dependent genes in the caudate putamen. (A) Volcano plot showing $\log_2$ fold change against $-\log_{10}$ *P*-value for the main effect of littermate control vs. *Slc30a10* knockout mice in the caudate putamen (CPu). Differentially expressed genes (DEGs) ($P_{adj} < 0.05$) are shown as blue dots. The top DEGs are labeled. (B) *Slc30a10* expression in the CPu of *Slc30a10* knockout (KO) or *Slc30a10*$^{fl/fl}$ littermate control mice. (C) Number of upregulated (598) and downregulated (246) DEGs in the CPu of *Slc30a10* knockout mice ($P_{adj} < 0.05$). Pathway enrichment and gene ontology analyses for upregulated CPu DEGs of *Slc30a10* knockout mice showing (D) major categories and (E) minor categories of enrichment as a function of $-\log_{10}$ (*P*-value). Pathway enrichment and gene ontology analyses for downregulated CPu DEGs of *Slc30a10* knockout mice showing (F) major categories and (G) minor categories of enrichment as a function of $-\log_{10}$ (*P*-value). $N = 4$ mice per genotype. Tissues were from the same mice used for Fig. 1. ****$P < 0.0001$.

neurotransmitter function, synaptic exocytosis, and membrane trafficking, including synaptotagmins and SNAREs (e.g. glutamate receptor *Grm2*, cholinergic receptor *Chrm3*, adrenergic receptor *Adra2a*, serotonin receptors *Htr1a* and *Htr2a*, synaptotagmins *Syt13* and *Syt17*, and the SNAREs *Stx1* and *Stx3*) (Table 1).[26] Expression of several HIF/hypoxia-regulated genes were also upregulated (Table 1).[26–29] Additionally, full-body *Slc30a10* knockouts also exhibit a hypothyroid phenotype induced by the accumulation of Mn in the thyroid, which blocks thyroxine synthesis[19,20] (subsequent to the discovery of hypothyroidism in *Slc30a10* knockout mice, hypothyroidism was reported in a human patient with *SLC30A10* mutations[33]). Consistent with this, we observed that expression of the thyroid hormone transporter *Slc7a5* was upregulated in the caudate putamen of the knockouts (Table 1).[26,34] Another characteristic change was upregulation of genes regulating Rho/RacGTPase pathways (Supplementary Tables S1 and S2). Notable downregulated genes and pathways included those mediating neurotransmitter release and secretion, synaptic transmission, and Ca-dependent exocytosis (e.g. glycine transporter *Slc6a9*, and synaptotagmins *Syt3* and *Syt9*) (Fig. 2F and G; Supplementary Tables S1 and S2),[26] and additionally, several metabolic pathways (Supplementary Tables S1 and S2). Thus, disruption in the expression of genes modulating synaptic/neurotransmitter function also occurs in the caudate putamen of the *Slc30a10* knockout mice.

Regulators of synaptic and neurotransmitter function are also differentially expressed in the globus pallidus of *Slc30a10* knockout mice

Expression of ∼350 genes were upregulated and ∼550 downregulated in the globus pallidus of the knockout strain (Fig. 3A–C; Supplementary Table S1). *Slc30a10* expression was again negligible in the knockouts (Fig. 3B; Supplementary Table S1). Upregulated pathways included numerous processes involved in synaptic organization and neuronal, axonal, and dendritic function (Fig. 3D and E; Supplementary Table S2). Notable genes with upregulated expression included *Stxbp5*, which codes for a syntaxin binding protein involved in SNARE function and neurotransmitter release, several hypoxia/HIF-regulated genes, and thyroid hormone transporters/regulators (Table 1).[26–29,34] Downregulated pathways and genes included several mediators of neuronal, glial, synaptic and neurotransmitter function (Fig. 3F and G; Supplementary Tables S1 and S2). Notable, specific downregulatory changes occurred in glutamatergic and GABAergic synaptic function (e.g. GABA transporter *Slc6a11* and ionotropic glutamate receptors *Grin3a* and *Gria4*) (Table 1). We also noted downregulatory changes in several metabolic pathways in the globus pallidus of the knockouts (Supplementary Tables S1 and S2). Thus, expression of genes modulating synaptic/neurotransmitter function are dysregulated in all three basal ganglia sub-regions of *Slc30a10* knockout mice.

Gene expression changes in the basal ganglia of *Slc30a10* knockout mice are sub-region specific

Next, we sought to identify genes/pathways that were similarly altered in all three basal ganglia sub-regions of *Slc30a10* knockout mice because these were likely critical homeostatic/adaptive or pathological responses to elevated Mn. Despite the widespread changes in expression in each individual basal ganglia region, expression of only 21 genes were upregulated and 7 downregulated in common in all three sub-regions (Fig. 4A and B; Supplementary Table S1). Expression of the hypoxia/HIF-regulated genes *Vegfa*, *Kdr*, and *Hif3a*[26–29] were among those upregulated in all three regions (Table 1, Supplementary Table S1), highlighting the centrality of HIF activation during Mn overload. While overlap in specific genes with altered expression in all three basal ganglia sub-regions was limited, overlap between alteration of pathways, including in pathways related to neuronal biology, was more evident (Fig. 4C and D). Overall, gene expression changes in *Slc30a10* knockout mice are influenced by the sub-region of the basal ganglia, but common themes in expression changes in hypoxia/HIF-dependent genes or genes regulating neurological function are evident throughout the basal ganglia.

A reduced Mn chow rescues majority of the gene expression changes in the basal ganglia of *Slc30a10* knockout mice

To test whether the gene/pathway expression changes in the basal ganglia of the *Slc30a10* knockouts were induced by elevated Mn, instead solely by loss of *Slc30a10* expression, we repeated the transcriptomic study in littermates and *Slc30a10* knockouts fed a reduced Mn chow containing ∼11 μg Mn/g chow. We previously reported that the reduced Mn chow significantly lowers the brain Mn content and rescues the motor deficits and hypothyroidism of the knockouts.[9,19] But, compared with littermates, brain Mn levels of the 6-wk-old knockouts on the reduced Mn chow are still ∼10-fold higher, compared with ∼40-fold difference between the genotypes on regular chow at this age.[19] Thus, we did not anticipate that gene expression changes in the knockouts on the reduced Mn chow would be fully normalized.

As expected, some gene and pathway expression changes occurred in each basal ganglia region of the *Slc30a10* knockouts on the reduced Mn chow (Fig. 5A–Q; Supplementary Tables S3 and S4). But, knockouts on the reduced Mn chow had a substantially lesser number of differentially expressed genes (DEGs)/pathways in each basal ganglia region compared with counterparts fed regular chow (compare Fig. 5 and Supplementary Tables S3 and S4 with Figs. 1–3 and Supplementary Tables S1 and S2). Furthermore, genes/pathways regulating neuronal function were not a major component of the expression changes that occurred in the basal ganglia sub-regions of the knockouts on the reduced Mn chow (Fig. 5D, E, I, J, N, and Q; Supplementary Tables S3 and S4). Only a few gene expression/pathway changes occurred in common in all three basal ganglia regions of the knockouts (Fig. 5O–Q). Notably, however, upregulation of expression of HIF/hypoxia-dependent genes persisted (Table 1), providing evidence of HIF activation in the basal ganglia of mice fed the reduced Mn chow. *Slc30a10* expression was negligible in each basal ganglia region of the knockouts fed the reduced Mn chow (Fig. 5B, G, and L), validating that the reduction in the gene/pathway expression changes in the knockouts was an effect of reducing the Mn content of chow and not an anomalous restoration of *Slc30a10* expression. Additional analyses revealed that the reduced Mn chow had a clear normalizing effect on the expression of most neuronal modulators observed in the knockouts fed regular rodent chow (Fig. 6A–E, see Fig. 6B in particular; and Supplementary Tables S5 and S6). Interestingly, some of the gene expression changes in the knockouts on the reduced chow were not observed with regular Mn chow (Supplementary Tables S5 and S6). The likely explanation is that varying brain Mn levels may have varying effects on gene expression. Overall, the main outcome of the rescue experiment is that the reduced Mn chow, which lowers brain Mn levels and rescues the motor phenotype of the *Slc30a10* knockouts,[9,19] also rescues differential expression of most genes/pathways in the

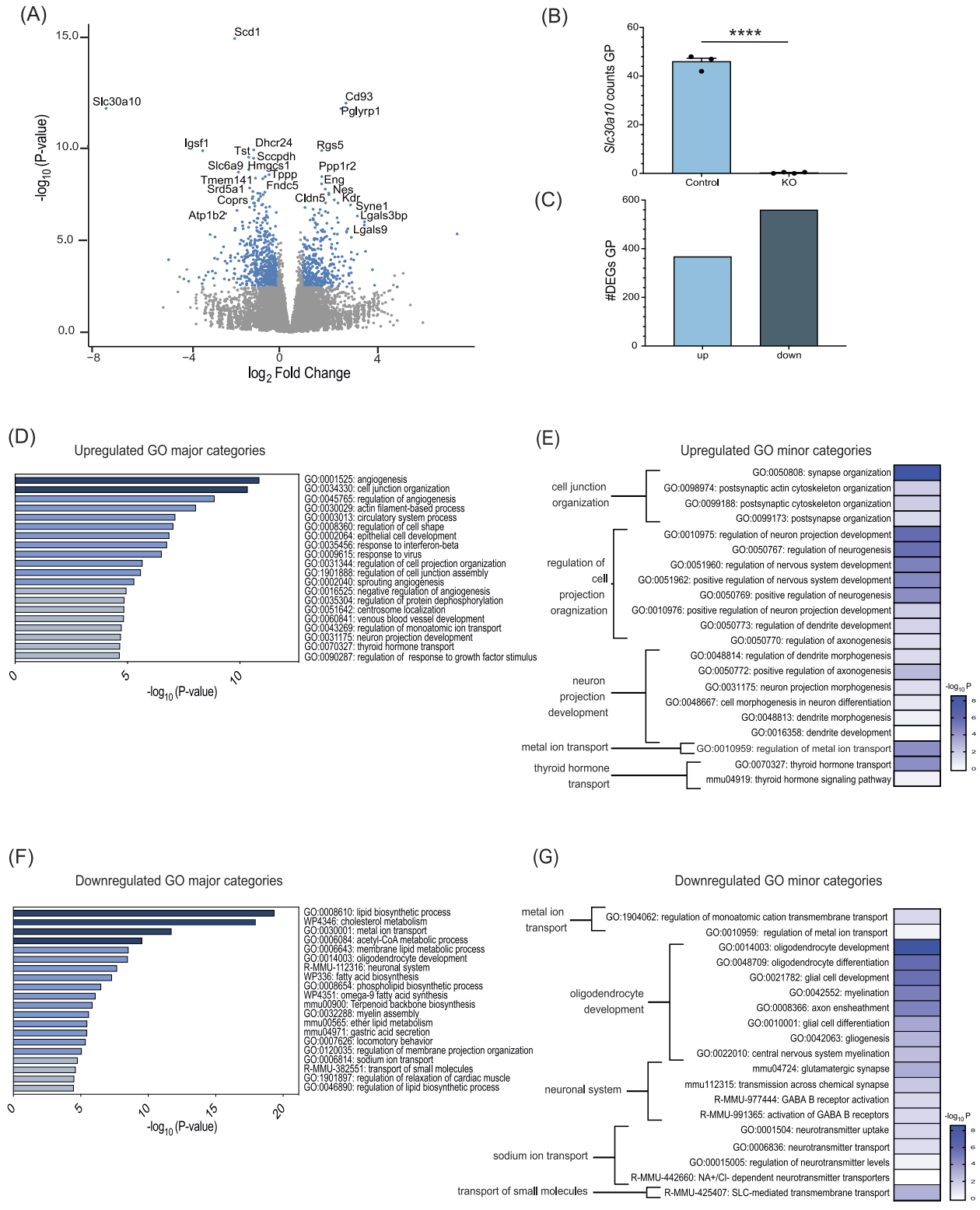

Fig. 3 Expression of neuronal regulators and HIF/hypoxia-dependent genes are also altered in the globus pallidus of *Slc30a10* knockout mice on regular rodent chow. (A) Volcano plot showing $\log_2$ fold change against $-\log_{10}$ *P*-value for the main effect of littermate control vs. *Slc30a10* knockout mice in the globus pallidus (GP). Differentially expressed genes (DEGs) ($P_{adj} < 0.05$) are shown as blue dots. The top DEGs are labeled. (B) Expression of *Slc30a10* in the GP of *Slc30a10* knockout (KO) or *Slc30a10*$^{fl/fl}$ littermate control mice. (C) Number of upregulated (367) and downregulated (560) DEGs in the GP of *Slc30a10* knockout mice ($P_{adj} < 0.05$). Pathway enrichment and gene ontology analyses for upregulated GP DEGs of *Slc30a10* knockout mice showing (D) major categories and (E) minor categories of enrichment as a function of $-\log_{10}$ (*P*-value). Pathway enrichment and gene ontology analyses for downregulated GP DEGs of *Slc30a10* knockout mice showing (F) major categories and (G) minor categories of enrichment as a function of $-\log_{10}$ (*P*-value). $N = 3$ littermate controls and 4 knockouts. Tissues were from the same mice used for Figs. 1 and 2. GP sample of one control mouse used in Figs. 1 and 2 was lost during processing; hence the sample size for the control genotype is 3 in this figure. ****$P < 0.0001$.

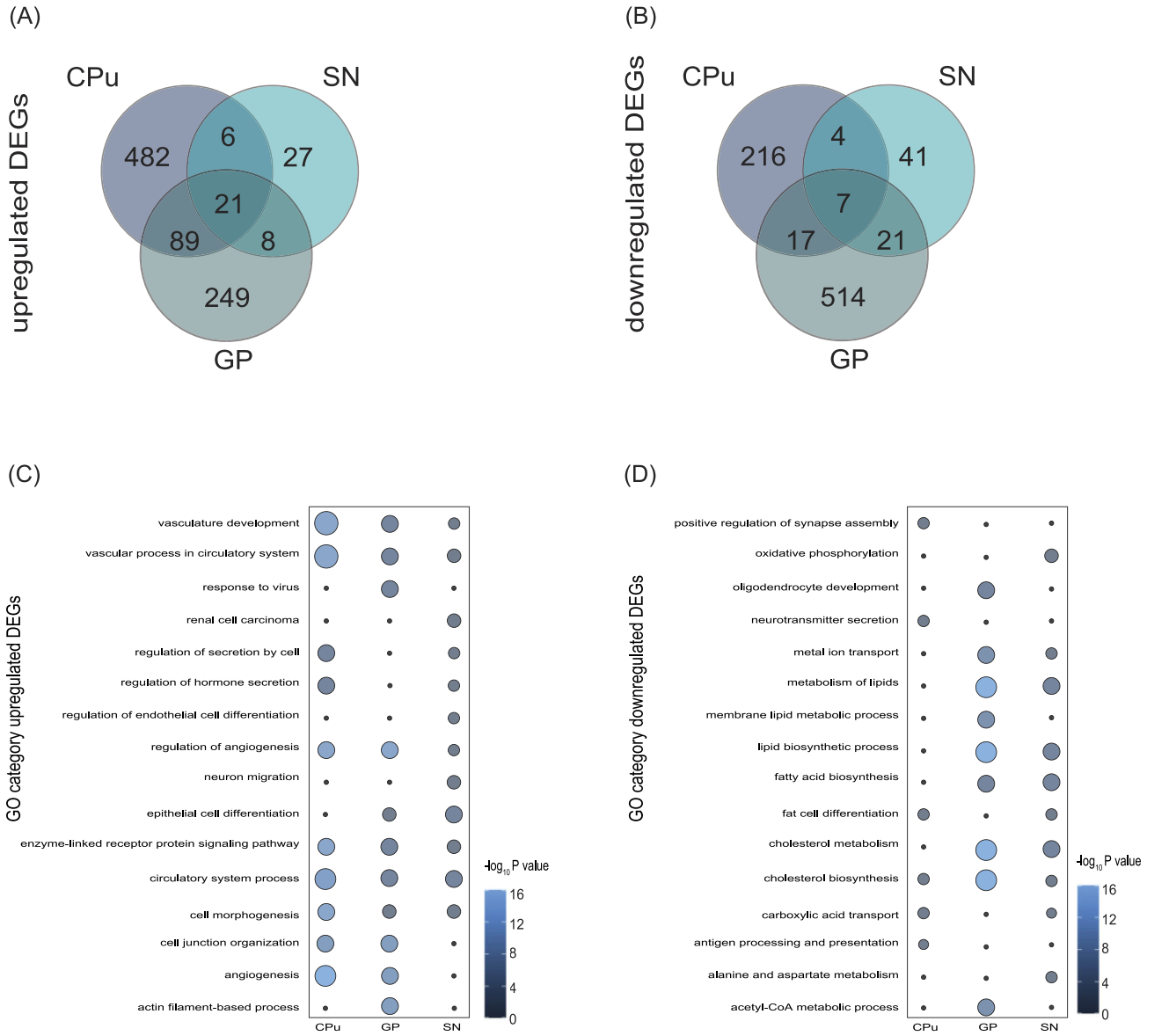

Fig. 4 Brain region specificity of gene expression changes in the basal ganglia of *Slc30a10* knockout mice on regular rodent chow. (A) Gene overlap of upregulated differentially expressed genes (DEGs) ($P_{adj} < 0.05$) between brain regions of *Slc30a10* knockout mice (SN—substantia nigra, GP—globus pallidus, CPu—caudate putamen). (B) Gene overlap of downregulated DEGs between brain regions. (C) Bubble plot visualization of the top pathway and gene ontology enrichments of upregulated DEGs between brain regions of *Slc30a10* knockout mice. Size and color of the bubble is a function of $-\log_{10}$ (*P*-value). (D) Bubble plot visualization of the top pathway and gene ontology enrichments of downregulated DEGs between brain regions. Size and color of the bubble is a function of $-\log_{10}$ (*P*-value).

basal ganglia of the knockouts, establishing that these expression changes are induced by Mn.

Activation of HIF signaling is a central feature of the transcriptomic response of *Slc30a10* knockout mice

From the prior data, activation of HIF signaling emerged as a central feature of the transcriptomic changes in the basal ganglia of the *Slc30a10* knockouts. As the final part of this study, we sought to further characterize the role of HIF signaling in gene/pathway expression changes observed in the *Slc30a10* knockouts. For this, we performed two sets of studies/analyses. First, we characterized gene/pathway expression changes in the liver of littermates or *Slc30a10* knockouts on regular or reduced Mn chow. The rationale for investigating expression changes in the liver was that: (i) in addition to the brain, SLC30A10 is also expressed in the liver (and intestines); and (ii) activity of SLC30A10 in the liver (and intestines) is fundamental in regulating brain Mn by mediating Mn excretion.[7–9] Second, we bioinformatically identified upstream regulators for the DEGs in the basal ganglia and the liver of the *Slc30a10* knockouts on regular or reduced Mn chow.

As expected, numerous genes and pathways were differentially expressed in the liver of *Slc30a10* knockout mice on regular or reduced Mn chow (Fig. 7A–J; Supplementary Tables S1–S4). Importantly, HIF/hypoxia-dependent genes were an important component of these expression changes with both diets (Supplementary Tables S2 and S4). Analyses of upstream regulators identified numerous transcription factors as regulators of the expression changes in the three basal ganglia sub-regions and the liver of the *Slc30a10* knockout mice (Fig. 8A–L). Importantly, signaling via HIF1 emerged as a central mediator of the

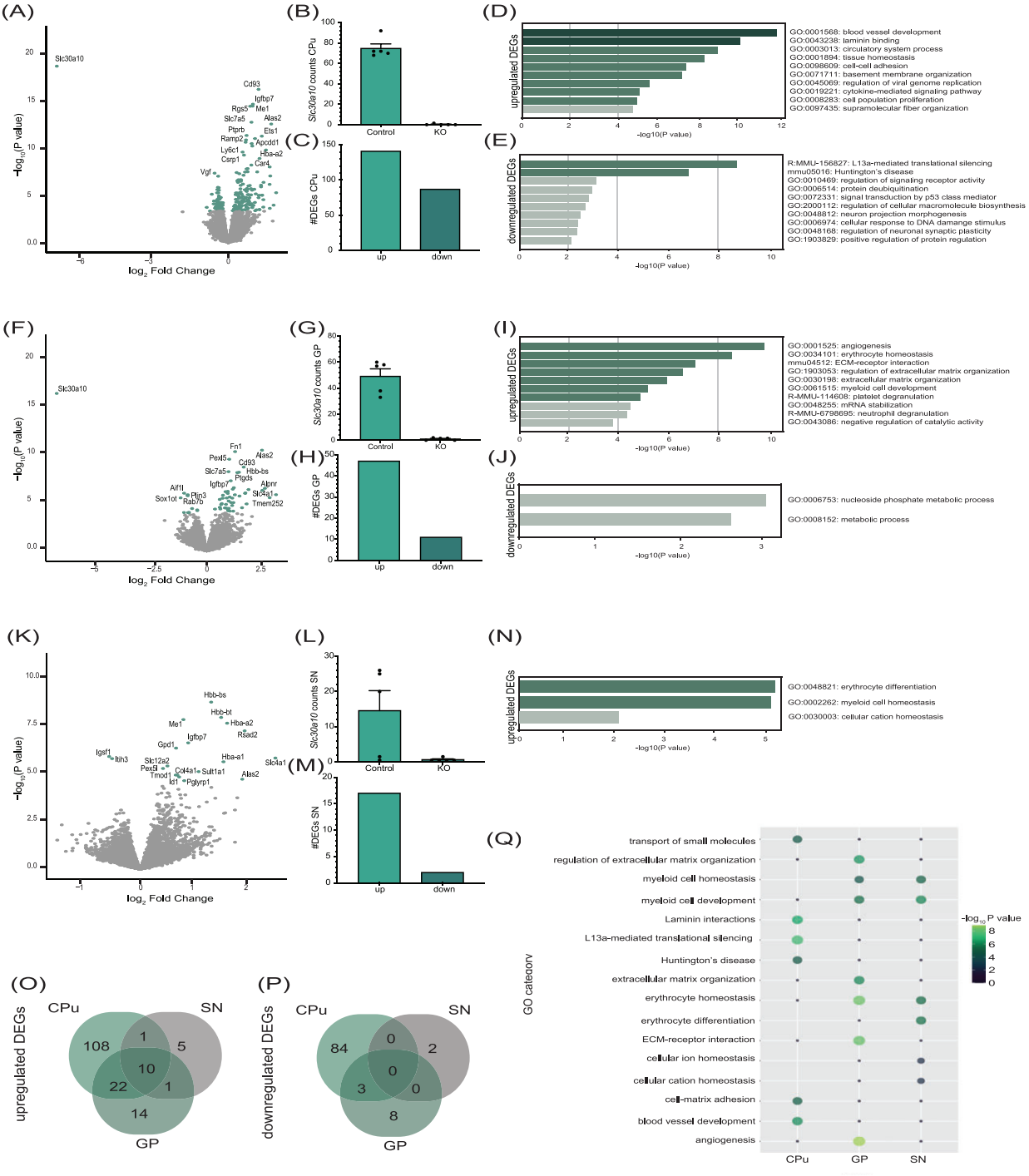

Fig. 5 Gene expression changes in the basal ganglia of *Slc30a10* knockout mice fed a reduced Mn chow. (A) Volcano plot showing $\log_2$ fold change against $-\log_{10}$ *P*-value for the main effect of littermate control vs. *Slc30a10* knockout mice in the caudate putamen (CPu). Differentially expressed genes (DEGs) ($P_{adj} < 0.05$) are shown as green dots. The top DEGs are labeled. (B) Expression of *Slc30a10* in *Slc30a10* knockout (KO) or littermate control mice in the CPu. (C) Number of upregulated (141) and downregulated (89) DEGs in the CPu of *Slc30a10* knockout mice ($P_{adj} < 0.05$). Pathway enrichment and gene ontology analyses for (D) upregulated CPu DEGs and (E) downregulated CPu DEGs of *Slc30a10* knockout mice as a function of $-\log_{10}$ (*P*-value). (F) Volcano plot showing $\log_2$ fold change against $-\log_{10}$ *P*-value for the main effect of littermate control vs. *Slc30a10* knockout mice in the globus pallidus (GP). DEGs ($P_{adj} < 0.05$) are shown as green dots. The top DEGs are labeled. (G) *Slc30a10* expression in *Slc30a10* knockout (KO) or littermate control mice in the GP. (H) Number of upregulated (47) and downregulated (11) DEGs in the GP ($P_{adj} < 0.05$). Pathway enrichment and gene ontology analyses for (I) upregulated GP DEGs and (J) downregulated GP DEGs of *Slc30a10* knockout mice as a function of $-\log_{10}$ (*P*-value). (K) Volcano plot showing $\log_2$ fold change against $-\log_{10}$ *P*-value for the main effect of littermate control vs. *Slc30a10* knockout mice in the substantia nigra (SN). DEGs ($P_{adj} < 0.05$) are shown as green dots. The top DEGs are labeled. (L) *Slc30a10* expression in *Slc30a10* knockout (KO) or littermate control mice in the SN. (M) Number of upregulated (17) and downregulated (2) DEGs in the SN ($P_{adj} < 0.05$). (N) Pathway enrichment and gene ontology analyses for upregulated SN DEGs of *Slc30a10* knockout mice as a function of $-\log_{10}$ (*P*-value). Gene overlap of (O) upregulated DEGs and (P) downregulated DEGs ($P_{adj} < 0.05$) between brain regions of *Slc30a10* knockout mice. (Q) Bubble plot visualization of the top pathway and gene ontology enrichments of DEGs between brain regions of *Slc30a10* knockout mice. Size and color of the bubble is a function of $-\log_{10}$ (*P*-value). $N = 5$ mice per genotype.

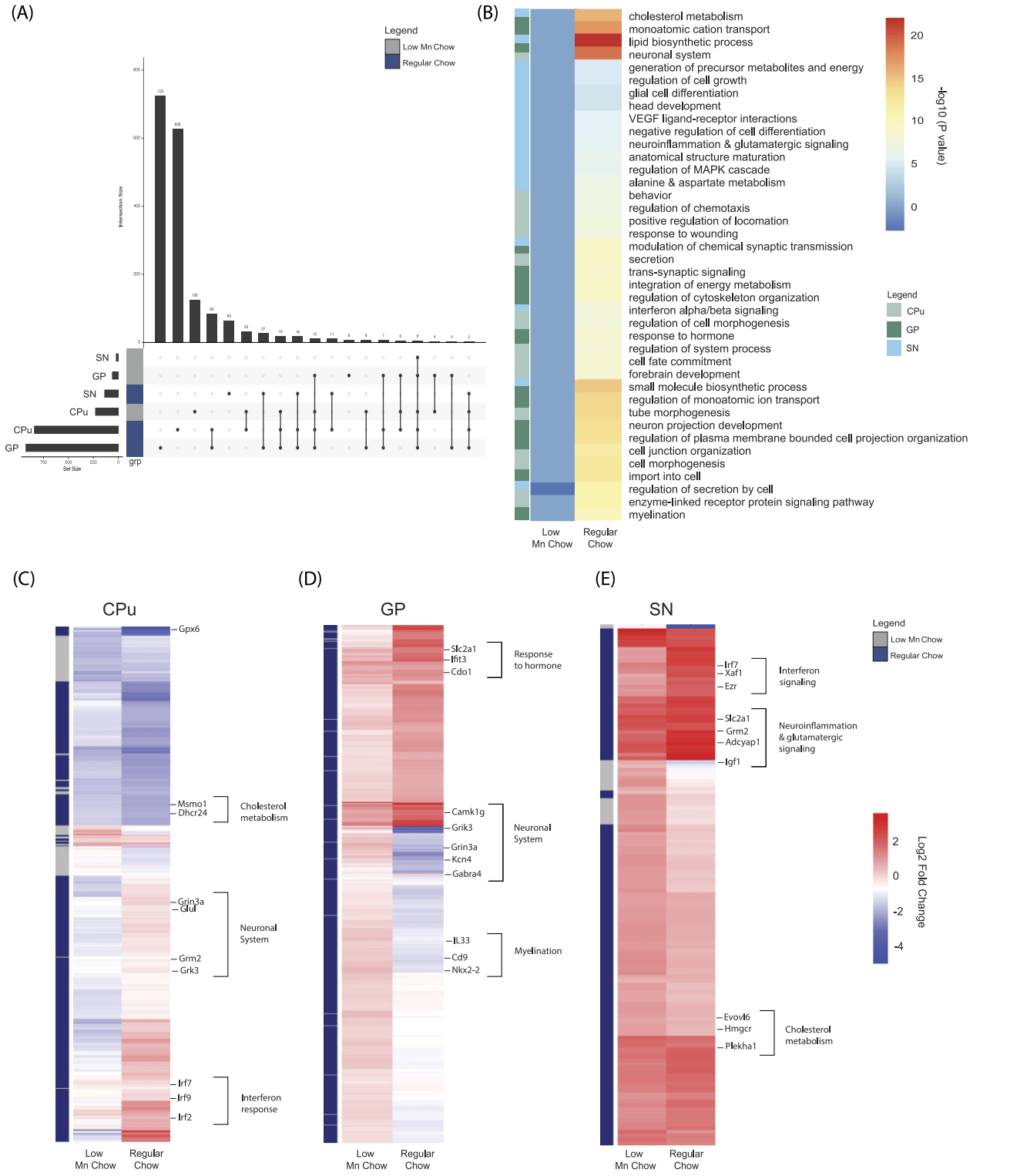

Fig. 6 Normalization effect of the reduced Mn chow in the basal ganglia of *Slc30a10* knockout mice. (A) UpSetR Plot visualizing the lack of differentially expressed genes (DEGs) overlap between brain regions of *Slc30a10* knockout mice fed reduced Mn (gray) or regular chow (blue), highlighting which gene expression changes are Mn dependent. Set size is plotted to the left of the chart, set membership is plotted above each bar, and each connection is highlighted as a connected line. (B) Heatmap of the top gene ontology and pathway enrichments of *Slc30a10* knockout mice fed regular rodent chow across brain regions (right) compared with enrichment of the same categories of *Slc30a10* knockout mice fed reduced Mn chow (left). Color is a function of $-\log_{10}$ (*P*-value), with dark blue representing no significant enrichment and warmer colors (light blue, yellow, orange, red) representing strong significant enrichment of the selected pathways in the dataset. Brain region metadata are represented on the left side bar as a function of color (light green—caudate putamen (CPu); dark green—globus pallidus (GP), light blue—substantia nigra (SN)). (C-E) To highlight the corrective effect, regular rodent chow specific DEGs of *Slc30a10* knockout mice were selected and plotted as heatmap for each brain region with reduced Mn chow on the left and regular rodent chow on the right. Specific DEGs and pathway categories are highlighted to demonstrate the normalization of Mn-dependent pathways. Color is a function of $\log_2$ fold change with blue representing downregulation and red representing upregulation of gene expression. All DEGs represented are ($P_{adj} < 0.05$). Chow metadata are represented on the left side bar as a function of color (gray—reduced Mn chow, blue—regular chow).

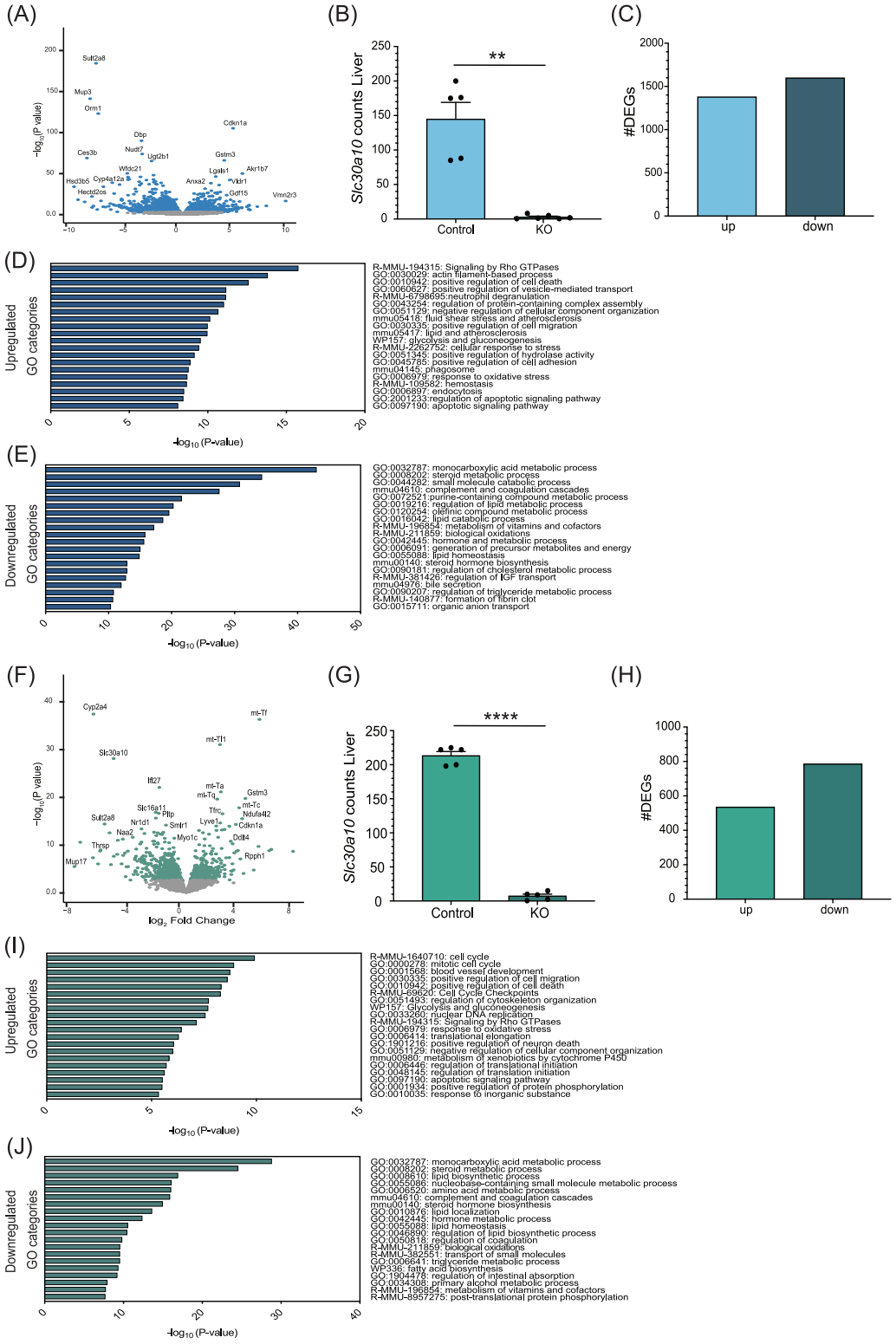

Fig. 7 Effect of regular or reduced Mn chow in the liver of *Slc30a10* knockout mice. (A) Volcano plot showing $\log_2$ fold change against $-\log_{10}$ *P*-value for the main effect of littermate control vs. *Slc30a10* knockout in the liver of mice fed regular rodent chow. Differentially expressed genes (DEGs) ($P_{adj} < 0.05$) are shown as blue dots. The top DEGs are labeled. (B) *Slc30a10* expression in the liver of *Slc30a10* knockout (KO) or *Slc30a10*$^{fl/fl}$ littermate control mice fed regular rodent chow. (C) Number of upregulated (1379) and downregulated (1598) DEGs in the liver of *Slc30a10* knockout mice ($P_{adj} < 0.05$) on regular rodent chow. Pathway enrichment and gene ontology analyses for (D) upregulated liver DEGs and (E) downregulated liver DEGs as a function of $-\log_{10}$ (*P*-value) of *Slc30a10* knockout mice fed regular rodent chow. (F) Volcano plot showing $\log_2$ fold change against $-\log_{10}$ *P*-value for the main effect of littermate control vs. *Slc30a10* knockout in the liver of mice on reduced Mn chow. DEGs ($P_{adj} < 0.05$) are shown as green dots. The top DEGs are labeled. (G) Liver *Slc30a10* expression in *Slc30a10* knockout (KO) or *Slc30a10*$^{fl/fl}$ littermate control mice fed reduced Mn chow. (H) Number of upregulated (535) and downregulated (788) DEGs in the liver ($P_{adj} < 0.05$) of *Slc30a10* knockout mice on reduced Mn chow. Pathway enrichment and gene ontology analyses for (I) upregulated liver DEGs and (J) downregulated liver DEGs as a function of $-\log_{10}$ (*P*-value) of *Slc30a10* knockout mice fed reduced Mn chow. $N = 5$–6 mice per genotype and diet. $^{**}P < 0.01$; $^{****}P < 0.0001$.

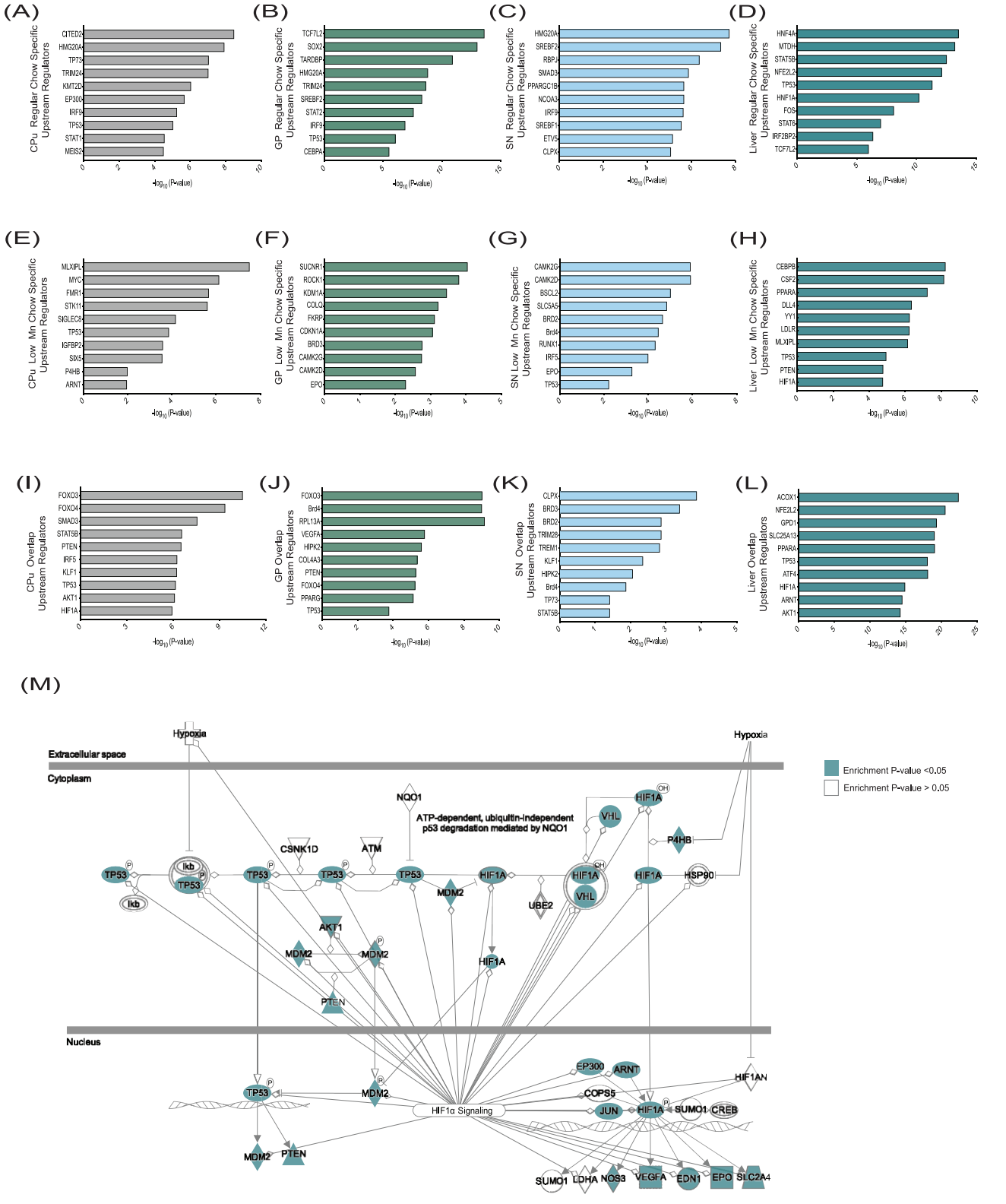

Fig. 8 Upstream regulator analysis highlights role for HIF1α signaling across organs and chows. Regular chow specific top upstream regulators enriched in the (A) caudate putamen (CPu), (B) globus pallidus (GP), (C) substantia nigra (SN), and (D) liver of *Slc30a10* knockout animals. Reduced Mn chow specific top upstream regulators enriched in the (E) CPu, (F) GP, (G) SN, and (H) liver of *Slc30a10* knockout animals. Reduced Mn and regular chow overlapping DEGs analysed for top upstream regulators enrichment in the (I) CPu, (J) GP, (K) SN, and (L) liver of *Slc30a10* knockout animals. (M) IPA pathway visualization of the HIF1α signaling pathway. Components that are enriched in the upstream regulator analyses across organs and chows are highlighted in blue, representing an enrichment $P_{adj} < 0.05$. Enrichment for each bar graph is a function of $-\log_{10}$ (*P*-value).

transcriptional response of the *Slc30a10* knockout mice (Fig. 8M). Note however that, while there are three HIF isoforms[27] (see Section "Discussion" for more details), the proprietary Ingenuity Pathway Analysis (IPA; QIAGEN, Redwood City, CA, USA) program used for pathway enrichment and upstream regulator analysis is limited to HIF1 and does not distinguish between HIF isoforms.[35] Consequently, we were unable to further segregate the upstream regulation of expression changes in the *Slc30a10* knockouts by HIF isoforms. But, irrespective of the role of specific HIF isoforms, our results imply that the HIF pathway is a major driver of the gene expression changes that occur in the basal ganglia and liver of *Slc30a10* knockout mice.

Discussion

The pervasive disruption in the expression of genes modulating neurotransmitter, synaptic, and neuronal function identified in the basal ganglia of the full-body *Slc30a10* knockout mice on regular rodent chow may contribute to the neuromotor phenotype evident in these animals. As brain Mn levels are markedly elevated in the full-body *Slc30a10* knockout mice at ~1 mo of age on regular rodent chow[9] when the mice were euthanized in this study, the expression changes we detected in the knockouts could be reflective of brain Mn increases at the time of euthanasia and/or at a prior developmental stage. An important next step in characterizing possible molecular mechanisms of neurological deficits in mice (and humans) lacking functional SLC30A10 is to use the current data for designing rescue studies that restore expression of select genes with altered expression in the *Slc30a10* knockout mice. It should be possible to prioritize genes for future mechanistic/rescue studies by comparing the basal ganglia transcriptomic profile of the full-body *Slc30a10* knockout mice (this study) with pan-neuronal/glial *Slc30a10* knockout mice, which is yet to be determined. Pan-neuronal/glial *Slc30a10* knockout mice: (i) lack SLC30A10 expression in neurons, astrocytes and oligodendrocytes[9,16] and (ii) under physiological conditions, exhibit modest, brain-region specific increases in Mn levels detectable only in early post-natal development along with lasting deficits in motor function and dopamine release that persist into adulthood.[16] Potentially, a similar comparative transcriptomics approach may also be used in the future with *Slc30a10* knockout strains and mice that have functional SLC30A10, but are exposed to human relevant Mn levels. Genes or gene expression pathways that exhibit similar alterations in full-body *Slc30a10* knockout mice, pan-neuronal/glial *Slc30a10* knockout mice, and Mn-treated mice with functional SLC30A10 may be central in the pathobiology of Mn-induced neuromotor disease. Because detectable brain Mn level increases in pan-neuronal/glial *Slc30a10* knockouts under physiological conditions are limited to early post-natal development,[16] it is likely that gene expression changes that emerge as critical modulators of the pathobiology of Mn neurotoxicity reflect lasting effects of early-life increases in brain Mn. Overall, while not mechanistic in itself, results of the current study are an important step in establishing the mechanisms of Mn-induced neurological disease.

The reduced Mn chow lowers, but does not fully normalize, brain Mn levels of full-body *Slc30a10* knockout mice.[19] Indeed, at ~6 wk of age, brain Mn levels of full-body knockouts on a reduced Mn chow are ~10-fold higher than littermates.[19] Yet, the reduced Mn chow rescues the motor deficits of the full-body knockouts (analyses at ~7–10 wk of age).[9] In contrast, as described earlier, pan-neuronal/glial *Slc30a10* knockouts fed regular rodent chow exhibit clear neuromotor deficits despite limited, transient, and region-specific increases in brain Mn (the only detectable change in brain Mn in the pan-neuronal/glial *Slc30a10* knockouts, compared with littermates, is ~40% increase in thalamus Mn at post-natal day 21).[16] The reasons underlying the contrasting motor phenotypes of the full-body *Slc30a10* knockouts on a reduced Mn chow and the pan-neuronal/glial *Slc30a10* knockouts are unclear, and may be informative about the relationship between brain Mn levels and motor dysfunction. For the current study, an implication is that the gene expression changes in the full-body *Slc30a10* knockout mice that were exclusive to the reduced Mn chow may not be related to the motor phenotype. Furthermore, gene expression changes that occurred in common with the two diets in the full-body *Slc30a10* knockouts, by themselves, may also be insufficient to drive motor deficits (because full-body *Slc30a10* knockout mice on the reduced Mn chow do not exhibit motor dysfunction[9]). But, the conserved expression changes that occurred with both diets may be sensitive responders to increases in Mn levels and/or critical contributors to the pathobiology of Mn-induced neurological disease. Analysing the role of these conserved gene expression changes in Mn neurotoxicity using directed approaches is another important direction for future work.

SLC30A10 is expressed in the brain, including in the basal ganglia, as well as in the liver and intestines.[8,9,16] SLC30A10 controls brain Mn levels by direct activity of brain SLC30A10, and additionally, by mediating hepatic and intestinal Mn excretion.[8,9,16] Using cell and mouse models of the liver and intestines, we recently established that the primary homeostatic response to elevated Mn levels is activation of HIF signaling, which transcriptionally upregulates SLC30A10 expression to reduce Mn levels and protect against Mn toxicity.[25] Our current findings indicate that: (i) HIF is also activated in the brain (i.e. basal ganglia) when brain Mn levels increase; and (ii) HIF activation is a major driver of the transcriptomic changes induced by elevated Mn levels in the basal ganglia and liver. Thus, together with our prior work,[25] the current results characterize activation of the HIF pathway to be a central feature of Mn level elevations in organs that are pathophysiologically important for Mn homeostasis and neurotoxicity.

HIFs are heterodimeric transcription factors formed by the dimerization of a labile α-subunit with a common and stable β-subunit.[27] Under normoxic conditions, the α-subunit undergoes prolyl hydroxylation, which targets it for degradation.[27] Mammals have three HIFα isoforms—HIF1α and HIF2α, which activate transcription after dimerization with the β-subunit,[27] and HIF3α, which has several splice variants including some that may inhibit HIF1α and HIF2α[27,29] (HIF heterodimers are named after the corresponding α-subunits). Our prior work established that Mn activates HIF signaling by inhibiting prolyl hydroxylation of the α-subunit,[25] and that HIF1α and HIF2α are redundant in controlling Mn homeostasis in cells.[25] But, whether HIFα isoforms play specific roles in modulating Mn homeostasis and neurotoxicity at the organism level is unknown and represents a critical direction for future work. As described earlier, due to the technical limitations with bioinformatic analyses,[35] the current findings do not shed light on potential roles of specific HIFα isoforms in driving the gene expression changes in *Slc30a10* knockout mice. Rigorous Mn exposure, neurobehavioral, and biochemical assays in isoform- and tissue-specific HIFα knockout mice will likely be necessary to define the isoform-specificity of HIFs in Mn homeostasis and neurotoxicity. These future studies will need to consider the possibilities that some Mn- and HIF-dependent genes may be mediating homeostatic protective responses to elevated Mn levels (e.g. *SLC30A10*) while others may contribute to the disease phenotype, and that the overall phenotype may be impacted by upregulation

of HIF3α, as observed in this study, which may inhibit HIF1α and HIF2α-mediated transcription.[27,29]

Methods

Knockout mouse strains

All experiments with mice were approved by the Institutional Animal Care and Use Committee of the University of Texas at Austin. We previously described the full-body *Slc30a10* knockout mice used here.[9,19,20] We used mice heterozygous for the knockout *Slc30a10* allele as breeders to get mice homozygous for the *Slc30a10* knockout allele (i.e. *Slc30a10*$^{-/-}$) or littermate control mice that were homozygous for the floxed *Slc30a10* allele (i.e. *Slc30a10*$^{fl/fl}$).We used male mice for this study because: (i) the Mn-induced hypothyroidism phenotype of male *Slc30a10*$^{-/-}$ mice is more severe than females[19]; and (ii) limiting the gene expression analyses to male mice enhanced the likelihood of identifying genotype-specific differences. Mice were housed in the specific-pathogen free facility of the University of Texas at Austin in a room maintained at 21°C with a 12 h light–dark cycle. Animals were weaned at post-natal day 21. After weaning, three to four littermates of the same sex were kept per cage. Animals had free access to food and water and were fed PicoLab Rodent Diet 20 with ~84 µg Mn/g chow.

We performed the reduced Mn diet rescue experiment exactly as described previously.[9,19] Briefly, on post-natal day 10, we changed diet of the dams to the commercially available reduced Mn chow, AIN-93 G, which contains ~11 μg Mn/g chow.[9,19] After weaning, pups continued to receive the reduced Mn chow until euthanasia.

Euthanasia and tissue collection

Mice were euthanized at ~1 mo of age by decapitation after isoflurane anesthesia as previously.[9,19] Liver and whole brain were isolated, flash-frozen in liquid nitrogen, and stored at −80°C before use. Brain punches were obtained essentially as described previously.[9,16] Brains were embedded in the O.C.T. Compound embedding medium (Scigen Scientific) and frozen on cold isopentane (Thermo Fisher Scientific). 500 µm coronal brain sections were sliced on a cryostat (set to ~−5°C). Desired brain regions were identified using the Allen Brain Reference Atlas (caudate putamen bregma coordinates: anteroposterior, 0.75 mm; mediolateral, 2 mm; dorsoventral, −3.5 mm; globus pallidus bregma coordinates: anteroposterior, −0.25 mm; mediolateral, 2 mm; dorsoventral, −4.5 mm; substantia nigra bregma coordinates: anteroposterior, −2.75 mm; mediolateral, 1.35 mm; dorsoventral, −5.5 mm). The targeted brain regions were collected with a brain punch tool (1.25 mm in diameter; Stoelting Co., Wood Dale, IL, USA). Bilateral punches per region were collected while the cryostat was set to −30°C. Tissue was kept frozen during the process.

Genotyping

This was also performed using previously described procedures.[9,19,20] Briefly, genomic DNA was extracted from tail snips using the Extracta DNA Prep for PCR—Tissue kit (Quanta Biosciences). PCR was performed using the AccuStart II PCR Supermix reagent (Quanta). Primers used were as follows: (i) to amplify the floxed *Slc30a10* allele—forward 5′ CGG ACT GGG AGC ACT TTG TT 3′, and reverse 5′ ATA CTG CCA CAG GAG AGG GG 3′; (ii) to amplify the knockout *Slc30a10* allele—forward 5′ CAC CTT TAA GGG CAC TAG GC 3′, and the reverse primer used for the floxed allele.

RNA extraction and sequencing

Total RNA from tissue was isolated using the PureLink RNA mini kit using manufacturer's instructions (Invitrogen). Genomic DNA was removed using RapidOut DNA Removal Kit (Thermo Fisher Scientific). Sequencing libraries were constructed using a 3′ Tag-based approach (TagSeq), targeting the 3′ end of mRNA fragments. This approach is a cost-efficient alternative to whole-transcriptome RNA sequencing, with comparable accuracy and quantification of transcripts.[36] The 3′ TagSeq was performed by the University of Texas Genomic Sequencing and Analysis Facility (RRID#: SCR_021713) based on the protocols from Lohman *et al.*[36] and Meyer *et al.*[37] Libraries were quantified using the Quant-it PicoGreen dsDNA assay (Thermo Fisher Scientific) and pooled equally for subsequent size selection at 350–550 bp on a 2% gel using the Blue Pippin (Sage Science). The final pools were checked for size and quality with the Bioanalyzer High Sensitivity DNA Kit (Agilent) and their concentrations were measured using the KAPA SYBR Fast qPCR kit (Roche). Samples were then sequenced on the NovaSeq 6000 (Illumina) instrument with single-end, 100 bp reads. Genes captured for the experiment with the regular rodent chow were 22,532 and for the experiment with the reduced Mn chow were 22,138.

Bioinformatics

Reads were mapped to the mouse reference genome (UCSC, GRCm39) using the alignment tool STAR (v2.7.10b). Raw RNA-sequencing files were evaluated for quality control using FastQC (v0.12.0). HTSeq (v.0.2.0) and Python (v.2.7) was used for counting mapped sequencing reads. RSeQC (v5.0.1) was used to further quality control mapped sequenced reads. Quantified read counts were normalized and analysed using DESeq2 (v1.12.3) to determine differential expression between groups, within the R statistical computing environment (v4.2.2).[38] Pairwise differential expression analyses were performed with DESeq2. Identical read filtering parameters were used for different organs, and genes with read counts <5 in at least half of the samples per treatment group were removed. DEGs are listed in Supplementary Tables S1 and S3. Genes with a nominal significance threshold of FDR <0.05 were used for further analysis. This threshold was selected to balance type 1 and type 2 error rates when performing pathway analyses. Normalized read counts were scaled according to the library size of individual samples. Functional enrichment of pathways and Gene Ontology categories was performed using Metascape.[39] Metascape combines functional enrichment, gene annotation, and membership within one integrated portal, minor categories are those that make up the major categories listed in Supplementary Tables S2 and S4 (orange = major, blue = minor). Significant enrichment was defined as a $-\log_{10}$ *P*-value >2 and a minimum of three genes per enrichment category. For upstream regulatory analysis (URA) of DEGs we used the commercial QIAGEN's IPA. For URA, we used the Bonferroni method to correct the detection *P*-value and set $P_{adj} < 0.05$ as the significant threshold as the input method. Pathway visualization was also performed using IPA (QIAGEN). Gene overlap to determine either brain regional specificity or regular vs. reduced Mn chow specificity was performed using GeneOverlap (v1.36.0, github.com/shenlab-sinai/GeneOverlap). Plots were generated using ggplot2 (v3.4.1), pheatmap (v1.0.12), UpSetR[40] or Prism (v9.01, GraphPad, San Diego, CA, USA).

Supplementary material

Supplementary data are available at *Metallomics* online.

Acknowledgements

TagSeq was performed by the Genomic Sequencing and Analysis Facility at UT Austin, Center for Biomedical Research Support (RRID#: SCR_021713).

Author contributions

C.L., K.C.G., and S.H. performed experiments. A.W. analyzed data and prepared figures. S.M., A.W., and R.D.M. interpreted data. S.M. and A.W. wrote the paper. R.D.M. commented on the paper. S.M. obtained funding.

Funding

Supported by National Institutes of Health/National Institute of Environmental Health Sciences grants R01-ES024812 and R01-ES031574 (both to S.M.).

Conflict of interest

Authors have no conflicts of interests to disclose.

Data availability

Sequencing data are available on the Gene Expression Omnibus (GEO) with accession ID GSE: GSE247882.

References

1. C. A. Taylor, K. Tuschl, M. M. Nicolai, J. Bornhorst, P. Gubert, A. M. Varao, M. Aschner, D. R. Smith and S. Mukhopadhyay, Maintaining Translational Relevance in Animal Models of Manganese Neurotoxicity, *J Nutr*, 2020, 150 (6), 1360–1369. https://doi.org/10.1093/jn/nxaa066
2. R. G. Lucchini, S. Guazzetti, S. Zoni, F. Donna, S. Peter, A. Zacco, M. Salmistraro, E. Bontempi, N. J. Zimmerman and D. R Smith, Tremor, Olfactory and Motor Changes in Italian Adolescents Exposed to Historical Ferro-Manganese Emission, *Neurotoxicology*, 2012, 33 (4), 687–696. https://doi.org/10.1016/j.neuro.2012.01.005
3. F. Rugless, A. Bhattacharya, P. Succop, K. N. Dietrich, C. Cox, J. Alden, P. Kuhnell, M. Barnas, R. Wright, P. J. Parsons, M. L. Praamsma, C. D. Palmer, C. Beidler, R. Wittberg and E. N Haynes, Childhood Exposure to Manganese and Postural Instability in Children Living Near a Ferromanganese Refinery in Southeastern Ohio, *Neurotoxicol Teratol*, 2014, 41:71–79. https://doi.org/10.1016/j.ntt.2013.12.005
4. L. Takser, D. Mergler, G. Hellier, J. Sahuquillo and G. Huel, Manganese, Monoamine Metabolite Levels at Birth, and Child Psychomotor Development, *Neurotoxicology*, 2003, 24 (4-5), 667–674. https://doi.org/10.1016/S0161-813X(03)00058-5
5. W. Liu, Y. Xin, Q. Li, Y. Shang, Z. Ping, J. Min, C. M. Cahill, J. T. Rogers and F. Wang, Biomarkers of Environmental Manganese Exposure and Associations with Childhood Neurodevelopment: a Systematic Review and Meta-Analysis, *Environ Health*, 2020, 19 (1), 104. https://doi.org/10.1186/s12940-020-00659-x
6. Y. Oulhote, D. Mergler, B. Barbeau, D. C. Bellinger, T. Bouffard, M. E. Brodeur, D. Saint-Amour, M. Legrand, S. Sauve and M. F. Bouchard, Neurobehavioral Function in School-Age Children Exposed to Manganese in Drinking Water, *Environ Health Perspect*, 2014, 122 (12), 1343–1350. https://doi.org/10.1289/ehp.1307918
7. K. C. Gurol, M. Aschner, D. R. Smith and S. Mukhopadhyay, Role of Excretion in Manganese Homeostasis and Neurotoxicity: a Historical Perspective, *Am J Physiol—Gastrointest Liver Physiol*, 2022, 322 (1), G79–G92. https://doi.org/10.1152/ajpgi.00299.2021
8. S. Hutchens, T. P. Jursa, A. Melkote, S. M. Grant, D. R. Smith and S. Mukhopadhyay, Hepatic and Intestinal Manganese Excretion Are Both Required to Regulate Brain Manganese during Elevated Manganese Exposure, *Am J Physiol—Gastrointest Liver Physiol*, 2023, 325 (3), G251–G264. https://doi.org/10.1152/ajpgi.00047.2023
9. C. A. Taylor, S. Hutchens, C. Liu, T. Jursa, W. Shawlot, M. Aschner, D. R. Smith and S. Mukhopadhyay, SLC30A10 Transporter in the Digestive System Regulates Brain Manganese under Basal Conditions While Brain SLC30A10 Protects against Neurotoxicity, *J Biol Chem*, 2019, 294 (6), 1860–1876. https://doi.org/10.1074/jbc.RA118.005628
10. K. Tuschl, P. T. Clayton, S. M. Gospe, Jr., S. Gulab, S. Ibrahim, P. Singhi, R. Aulakh, R. T. Ribeiro, O. G. Barsottini, M. S. Zaki, M. L. Del Rosario, S. Dyack, V. Price, A. Rideout, K. Gordon, R. A. Wevers, W. K. Chong and P. B Mills, Syndrome of Hepatic Cirrhosis, Dystonia, Polycythemia, and Hypermanganesemia Caused by Mutations in SLC30A10, a Manganese Transporter in Man, *Am Hum Genet*, 2012, 90 (3), 457–466. https://doi.org/10.1016/j.ajhg.2012.01.018
11. K. Tuschl, E. Meyer, L. E. Valdivia, N. Zhao, C. Dadswell, A. Abdul-Sada, C. Y. Hung, M. A. Simpson, W. K. Chong, T. S. Jacques, R. L. Woltjer, S. Eaton, A. Gregory, L. Sanford, E. Kara, H. Houlden, S. M. Cuno, H. Prokisch, L. Valletta, V. Tiranti, R. Younis, E. R. Maher, J. Spencer, A. Straatman-Iwanowska, P. Gissen, L. A. Selim, G. Pintos-Morell, W. Coroleu-Lletget, S. S. Mohammad, S. Yoganathan, R. C. Dale, M. Thomas, J. Rihel, O. A. Bodamer, C. A. Enns, S. J. Hayflick, P. T. Clayton, P. B. Mills, M. A. Kurian and S. W. Wilson, Mutations in SLC39A14 Disrupt Manganese Homeostasis and Cause Childhood-Onset Parkinsonism-Dystonia, *Nat Commun*, 2016, 7:1, 11601. https://doi.org/10.1038/ncomms11601
12. M. Quadri, A. Federico, T. Zhao, G. J. Breedveld, C. Battisti, C. Delnooz, L. A. Severijnen, L. Di Toro Mammarella, A. Mignarri, L. Monti, A. Sanna, P. Lu, F. Punzo, G. Cossu, R. Willemsen, F. Rasi, B. A. Oostra, B. P. van de Warrenburg and V. Bonifati, Mutations in SLC30A10 Cause Parkinsonism and Dystonia with Hypermanganesemia, Polycythemia, and Chronic Liver Disease, *Am Hum Genet*, 2012, 90 (3), 467–477. https://doi.org/10.1016/j.ajhg.2012.01.017
13. C. R. Gerfen and D. J. Surmeier, Modulation of Striatal Projection Systems by Dopamine, *Annu Rev Neurosci*, 2011, 34, 441–466. https://doi.org/10.1146/annurev-neuro-061010-113641
14. J. A. Obeso, M. C. Rodriguez-Oroz, B. Benitez-Temino, F. J. Blesa, J. Guridi, C. Marin and M. Rodriguez, Functional Organization of the Basal Ganglia: Therapeutic Implications for Parkinson's Disease, *Mov Disord*, 2008, 23 (S3), S548–S559. https://doi.org/10.1002/mds.22062
15. J. M. Gorell, C. C. Johnson, B. A. Rybicki, E. L. Peterson, G. X. Kortsha, G. G. Brown and R. J. Richardson, Occupational Exposure To Manganese, Copper, Lead, Iron, Mercury and Zinc and the Risk of Parkinson's Disease, *Neurotoxicology*, 1999, 20 (2-3), 239–247.
16. C. A. Taylor, S. M. Grant, T. Jursa, A. Melkote, R. Fulthorpe, M. Aschner, D. R. Smith, R. A. Gonzales and S. Mukhopadhyay, SLC30A10 Manganese Transporter in the Brain Protects against Deficits in Motor Function and Dopaminergic Neurotransmission under Physiological Conditions, *Metallomics*, 2023, 15 (4), mfad021. https://doi.org/10.1093/mtomcs/mfad021

17. A. N. Rodichkin, M. K. Edler, J. L. McGlothan and T. R. Guilarte, Behavioral and Neurochemical Studies of Inherited Manganese-Induced Dystonia-Parkinsonism in Slc39a14-Knockout Mice, *Neurobiol Dis*, 2021, 158, 105467. https://doi.org/10.1016/j.nbd.2021.105467
18. S. M. Lasley, C. A. Fornal, S. Mandal, B. J. Strupp, S. A. Beaudin and D. R. Smith, Early Postnatal Manganese Exposure Reduces Rat Cortical and Striatal Biogenic Amine Activity in Adulthood, *Toxicol Sci*, 2020, 173 (1), 144–155. https://doi.org/10.1093/toxsci/kfz208
19. S. Hutchens, C. Liu, T. Jursa, W. Shawlot, B. K. Chaffee, W. Yin, A. C. Gore, M. Aschner, D. R. Smith and S. Mukhopadhyay, Deficiency in the Manganese Efflux Transporter SLC30A10 Induces Severe Hypothyroidism in Mice, *J Biol Chem*, 2017, 292 (23), 9760–9773. https://doi.org/10.1074/jbc.M117.783605
20. C. Liu, S. Hutchens, T. Jursa, W. Shawlot, E. V. Polishchuk, R. S. Polishchuk, B. K. Dray, A. C. Gore, M. Aschner, D. R. Smith and S. Mukhopadhyay, Hypothyroidism Induced by Loss of the Manganese Efflux Transporter SLC30A10 May Be Explained by Reduced Thyroxine Production, *J Biol Chem*, 2017, 292 (40), 16605–16615. https://doi.org/10.1074/jbc.M117.804989
21. D. Leyva-Illades, P. Chen, C. E. Zogzas, S. Hutchens, J. M. Mercado, C. D. Swaim, R. A. Morrisett, A. B. Bowman, M. Aschner and S. Mukhopadhyay, SLC30A10 Is a Cell Surface-Localized Manganese Efflux Transporter, and Parkinsonism-Causing Mutations Block Its Intracellular Trafficking and Efflux Activity, *J Neurosci*, 2014, 34 (42), 14079–14095. https://doi.org/10.1523/JNEUROSCI.2329-14.2014
22. C. E. Zogzas, M. Aschner and S. Mukhopadhyay, Structural Elements in the Transmembrane and Cytoplasmic Domains of the Metal Transporter SLC30A10 Are Required for Its Manganese Efflux Activity, *J Biol Chem*, 2016, 291 (31), 15940–15957. https://doi.org/10.1074/jbc.M116.726935
23. C. E. Zogzas and S. Mukhopadhyay, Putative metal Binding Site in the Transmembrane Domain of the Manganese Transporter SLC30A10 Is Different from that of Related Zinc Transporters, *Metallomics*, 2018, 10 (8), 1053–1064. https://doi.org/10.1039/C8MT00115D
24. C. J. Mercadante, M. Prajapati, H. L. Conboy, M. E. Dash, C. Herrera, M. A. Pettiglio, L. Cintron-Rivera, M. A. Salesky, D. B. Rao and T. B. Bartnikas, Manganese Transporter Slc30a10 Controls Physiological Manganese Excretion and Toxicity, *J Clin Invest*, 2019, 129 (12), 5442–5461. https://doi.org/10.1172/JCI129710
25. C. Liu, T. Jursa, M. Aschner, D. R. Smith and S. Mukhopadhyay, Up-Regulation of the Manganese Transporter SLC30A10 by Hypoxia-Inducible Factors Defines a Homeostatic Response to Manganese Toxicity, *Proc. Natl. Acad. Sci. U.S.A.*, 2021, 118 (35). https://doi.org/10.1073/pnas.2107673118
26. Gene [Internet]. Bethesda (MD): National Library of Medicine (US), National Center for Biotechnology Information; 2004—2024. Available from: https://www.ncbi.nlm.nih.gov/gene/
27. A. J. Majmundar, W. J. Wong and M. C. Simon, Hypoxia-Inducible Factors and the Response to Hypoxic Stress, *Mol Cell*, 2010, 40 (2):294–309. https://doi.org/10.1016/j.molcel.2010.09.022
28. J. Waltenberger, U. Mayr, S. Pentz and V. Hombach, Functional Upregulation of the Vascular Endothelial Growth Factor Receptor KDR by Hypoxia, *Circulation*, 1996, 94 (7), 1647–1654. https://doi.org/10.1161/01.cir.94.7.1647
29. C. Duan, Hypoxia-Inducible Factor 3 Biology: Complexities and Emerging Themes, *Am J Physiol—Cell Physiol*, 2016, 310 (4), C260–C269. https://doi.org/10.1152/ajpcell.00315.2015
30. C. Chen, N. Pore, A. Behrooz, F. Ismail-Beigi and A. Maity, Regulation of Glut1 mRNA by Hypoxia-Inducible Factor-1. Interaction between H-ras and Hypoxia, *J Biol Chem*, 2001, 276 (12), 9519–9525. https://doi.org/10.1074/jbc.M010144200
31. M. Koshiji, Y. Kageyama, E. A. Pete, I. Horikawa, J. C. Barrett and L. E. Huang, HIF-1alpha Induces Cell Cycle Arrest by Functionally Counteracting Myc, *EMBO J*, 2004, 23 (9), 1949–1956. https://doi.org/10.1038/sj.emboj.7600196
32. A. R. Dunn, K. A. Stout, M. Ozawa, K. M. Lohr, C. A. Hoffman, A. I. Bernstein, Y. Li, M. Wang, C. Sgobio, N. Sastry, H. Cai, W. M. Caudle and G. W. Miller, Synaptic Vesicle Glycoprotein 2C (SV2C) Modulates Dopamine Release and Is Disrupted in Parkinson Disease, *Proc. Natl. Acad. Sci. U.S.A.*, 2017, 114 (11), E2253–E2E62. https://doi.org/10.1073/pnas.1616892114
33. S. Anagianni and K. Tuschl, Genetic Disorders of Manganese Metabolism, *Curr Neurol Neurosci Rep*, 2019, 19 (6), 33. https://doi.org/10.1007/s11910-019-0942-y
34. E. K. Wirth, U. Schweizer and J. Kohrle, Transport of Thyroid Hormone in Brain, *Front. Endocrinol.*, 2014, 5, 98. https://doi.org/10.3389/fendo.2014.00098
35. A. Kramer, J. Green, J. Pollard, Jr. and S. Tugendreich, Causal Analysis Approaches in Ingenuity Pathway Analysis, *Bioinformatics*, 2014, 30 (4), 523–530. https://doi.org/10.1093/bioinformatics/btt703
36. B. K. Lohman, J. N. Weber and D. I. Bolnick, Evaluation of TagSeq, a Reliable Low-Cost Alternative for RNAseq, *Mol Ecol Resour*, 2016, 16 (6), 1315–1321. https://doi.org/10.1111/1755-0998.12529
37. E. Meyer, G. V. Aglyamova and M. V. Matz, Profiling Gene Expression Responses of Coral Larvae (*Acroporamillepora*) to Elevated Temperature and Settlement Inducers Using a Novel RNA-Seq Procedure, *Mol Ecol*, 2011, 20 (17), 3599–3616. https://doi.org/10.1111/j.1365-294X.2011.05205.x
38. M. I. Love, W. Huber and S. Anders, Moderated Estimation of Fold Change and Dispersion for RNA-seq Data with DESeq2, *Genome Biol*, 2014, 15 (12), 550. https://doi.org/10.1186/s13059-014-0550-8
39. Y. Zhou, B. Zhou, L. Pache, M. Chang, A. H. Khodabakhshi, O. Tanaseichuk, C. Benner and S. K. Chanda, Metascape Provides a Biologist-Oriented Resource for the Analysis of Systems-Level Datasets, *Nat Commun*, 2019, 10 (1), 1523. https://doi.org/10.1038/s41467-019-09234-6
40. J. R. Conway, A. Lex and N. Gehlenborg, UpSetR: an R Package for the Visualization of Intersecting Sets and Their Properties, *Bioinformatics*, 2017, 33 (18), 2938–2940. https://doi.org/10.1093/bioinformatics/btx364

Received: October 10, 2023. **Accepted:** January 16, 2024